Multibody Approach to the Controlled Removal of Large Space Debris with Flexible Appendages

Singh, Sunayna; Mooij, Erwin; Gransden, Derek I.

DOI
10.2514/6.2019-1916

Publication date
2019

Document Version
Final published version

Published in
AIAA Scitech 2019 Forum

Multibody Approach to the Controlled Removal of Large Space Debris with Flexible Appendages

Sunayna Singh* and Erwin Mooij†
Delft University of Technology, Faculty of Aerospace Engineering,
Kluyverweg 1, 2629 HS Delft, The Netherlands

Derek I. Gransden‡
Laurentian University, Bharti School of Engineering
935 chemin du Lac Ramsey Lake Road, Sudbury, ON P3E2C6, Canada

The space environment is ever-changing with the space structures getting larger and the orbits getting increasingly crowded with time. This creates a need for removal of large defunct satellites to avoid the disastrous Kessler syndrome, which poses a major threat to the future of space exploration. This paper examines the dynamics and control involved in the active removal of a large space debris - Envisat. European Space Agency's e.deorbit mission aims to de-orbit Envisat using a chaser satellite, which synchronises, docks, detumbles and deorbits it. The presence of large flexible appendages make the configuration prone to elastic perturbations leading to complex dynamics that cannot be represented using rigid body dynamics. Therefore, a unique multibody approach based on the absolute interface coordinates in the floating frame formulation is used to model the Flexible Multibody Dynamics. The new method proves to provide a good balance between computation time and efficiency for the control application. The controllability characteristics of two phases of the e.deorbit mission are analysed using a linear PD controller and an Incremental Nonlinear Dynamic Inversion controller. For the first phase, both controllers successfully synchronise the chaser with the target debris tumbling at the rate of 3.5 $^\circ/s$ about all axes. However, during the detumbling phase, the large appendage (14.2 m) in the stacked configuration introduces complex dynamics, which could not be stabilised by applied controllers.

I. Introduction

Over the past decades, space structures have become larger, and with the increasing power requirements, they entail large solar panels. This has brought a diverse set of challenges to the field of spacecraft attitude dynamics and control. Spacecraft with smaller appendages are often modelled as rigid bodies due to their relatively dominant rigid properties. However, large appendages can cause considerable disturbing torques due to vibration, leading to instabilities in the system and cannot be modelled as rigid bodies. Assuming a rigid configuration for long appendages can also overlook important physical properties, like the vibrational and rotational coupling of the rigid and flexible elements. This might lead to faulty models, which can be potentially catastrophic. Hence, the Flexible Multibody Dynamics (FMD) of the system becomes crucial in such cases. The study of large flexible multibody space systems includes dynamics associated with assembly and docking of large space structures, deployment and retrieval of appendages, slew manoeuvres and

*MSc Student, Section Astrodynamics and Space Missions, sunayna.hima.9@gmail.com
†Assistant Professor, section Astrodynamics and Space Missions, e.mooij@tudelft.nl, Associate Fellow AIAA.
‡Master Lecturer, Bharti School of Engineering, dgransden@laurentian.ca

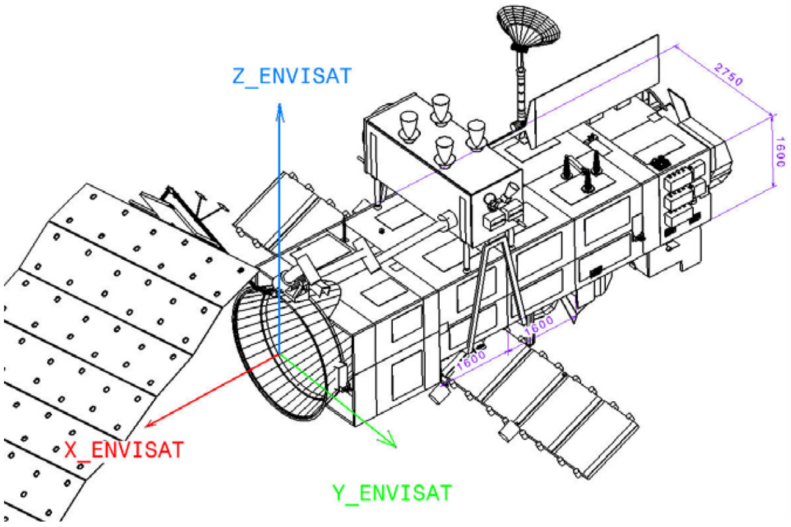

Figure 1. Stacked configuration of Envisat (bottom) and Chaser (top) (Credits:ESA)

precision pointing, and lately, active removal of space debris, all to be controlled in the presence of disturbing environmental forces. In this research, a unique multibody approach based on floating reference frames,[1] which enables modelling of constraints in a multibody system without the use of Lagrange multipliers, will be used. The new method facilitates modelling of the system's degrees of freedom through absolute interface coordinates between any two bodies in the multibody configuration. Further, it also allows modal reduction, which reduces the computation time considerably.

With the increasing number of satellites launched every year, the problem of accumulating space debris cannot be overlooked. While it is possible to avoid collision of the active satellites, the inactive large debris still remain uncontrolled and cause constant threat of collision with each other to further increase the debris population. The European Space Agency (ESA) suggests an order of 5-10 large objects to be removed to sustain the current scenario and avoid the devastating Kessler Syndrome[a]. This can be achieved through Active Debris Removal (ADR) techniques using different mechanisms, like tethers, throw-nets, harpoon, tentacles or clamps, depending on the size of the debris. Among all options stated here, a chaser satellite with tentacles and robotic arm to capture the target debris is among the most promising ones in the light of ESA's e.deorbit mission. The mission aims at removing Envisat, a large eight tonne defunct Earth Observation Satellite with a 14.2 m long solar array, which lost contact on April, 2012, after 10 years of successful operation. The debris now poses the highest collision risk of all ESA owned satellites in the densely populated altitude of 600-800 km near polar orbit. Through remote observations performed in 2013, it was found that the debris is rotating counter-clockwise at a rate of 3.5°/s about its Z-axis (radial direction), and with smaller rates about the other axes. The large mass, large appendage (approximately 14.2 m) and complex capture access due to uncontrollable tumbling and large flexible appendages make it an ideal case study for the application of the new multibody modelling approach to ADR techniques.

The deorbiting of Envisat can be undertaken in three phases : the synchronisation phase, the semi-connected phase, and the connected phase. The chaser first synchronises with the attitude of the tumbling uncooperative target. In the second phase, the chaser docks with the target using tentacles and/or a robotic arm. The contact is achieved between the target and chaser, but a rigid connection is not established yet. The system is connected by flexible links and prone to additional torques due to attitude differences. In the third and final phase, a more rigid connection is established and the stacked configuration is achieved as shown in Fig. 1. The system consists of combined mass and inertia properties and the chaser makes manoeuvres to stabilise the stacked system. The presence of large flexible appendages and multiple bodies stacked into one configuration, characterises a non-linear flexible multibody problem. In this research, only the synchronisation and connected phase will be analysed.

Clearly, the mission not only requires state-of-the-art sensors, but also a very robust control system to perform autonomous rendezvous and docking operations. Envisat's uncontrolled attitude and presence of

[a]https://www.esa.int/Our_Activities/Operations/Space_Debris/Active_debris_removal, last accessed : June 1, 2018

multiple flexible appendages make it prone to additional perturbations caused by the vibration of the flexible elements. The dynamics associated with the asymmetrical mass, geometry and flexibility properties of the stacked configuration is also very intriguing. The capabilities of two controllers, i.e., a linear PD controller and a nonlinear feedback controller, Incremental Nonlinear Dynamic Inversion (INDI), will be analysed. The system will also be modelled as a rigid system to compare and understand how the structural dynamics affects the controllability characteristics. To summarise, the research will examine the integrated dynamics and control of synchronisation of a chaser satellite with a large tumbling debris and, detumbling the docked configuration with flexible elements, with the dynamics modelled using a unique multibody approach based on floating frames. A detailed description of the research can be found in Ref. 2.

In this paper, Sec. II defines the requirement from the FMD model. The equations of motion (EOM) for the flexible system are also derived in this section. Lastly, the model is verified and validated using two test cases. This is followed up by the structural modelling strategy to adapt the satellite model to the new dynamic formulation in Sec. III. Sec. IV provides a brief description of rigid body dynamics for the guidance system. Also, the theory for the two controllers used in the research is discussed. In Sec. V, the results from the control two phases of e.deorbit mission are presented and analysed. Section VI concludes the paper and provides some recommendations.

II. Flexible Multibody Dynamics

The term Flexible Multibody Dynamics (FMD) refers to computational methods used to determine the dynamic response of a group of interconnected bodies (rigid or flexible), undergoing large translational and/or rotational motion. However, the essence of modelling of a complex Flexible Multibody System (FMS) with asymmetric mass and geometry (as it is in the current configuration), lies in careful selection of a number of aspects. This includes mindful choice of a reference frame formulation, constraint handling techniques, model reduction, internal forces, design of the FMS, and solution techniques. In this section, these aspects will be discussed briefly, and the suitability of the new method for the application will be explained. Based on the application of control of a large tumbling space debris, a number of requirements can be set up for the dynamic model,

1. The model should be computationally fast to be able to analyse the effect of multiple controller designs and different operational aspects on the system's stability characteristics within a feasible time frame.

2. The model should account for the effect of elastic dynamics of the system in sufficient detail. For instance, the level of detail and accuracy should be such that the effect of small, discrete control-moment changes are appropriately captured.

3. The model should allow easy constraint handling, because the configuration is changing with different phases of the mission.

A. Reference Frame Formulation

To reduce the simulation time and to capture the vibrational motion of the flexible appendages, the effect of deformation can be approximated by superimposing small linear vibrations on the rigid body motion, also called mean rigid body motion. So, the formulation should be such that the resulting EOM can define the mean rigid body motion of the system, when exposed to large rotations. Three essentially different, but commonly used formulations in FMD reference frame are: the inertial formulation, the co-rotational formulation, and the floating frame formulation, as shown in Fig. 2 with the respective frames highlighted in red. Most modern multibody formulations (for example, the absolute nodal formulation) are built around these three methods.

The *inertial frame formulation* defines the motion of the FMS with respect to the central body, which in this case is Earth. It is derived from the non-linear Finite Element Method (FEM) and continuum mechanics, wherein each body is discretised into a finite mesh, as shown in Fig. 2(a). The degrees of freedom (DOF) of such a system are defined by absolute position and orientation of the local coordinate frames at the nodes of the discretised body. The *co-rotational frame formulation* is defined as a non-linear extension of the linear FEM formulation. This formulation is derived from the field of structural dynamics, wherein the (large) rigid body motion is defined with respect to the inertial frame, and small elastic deformations in

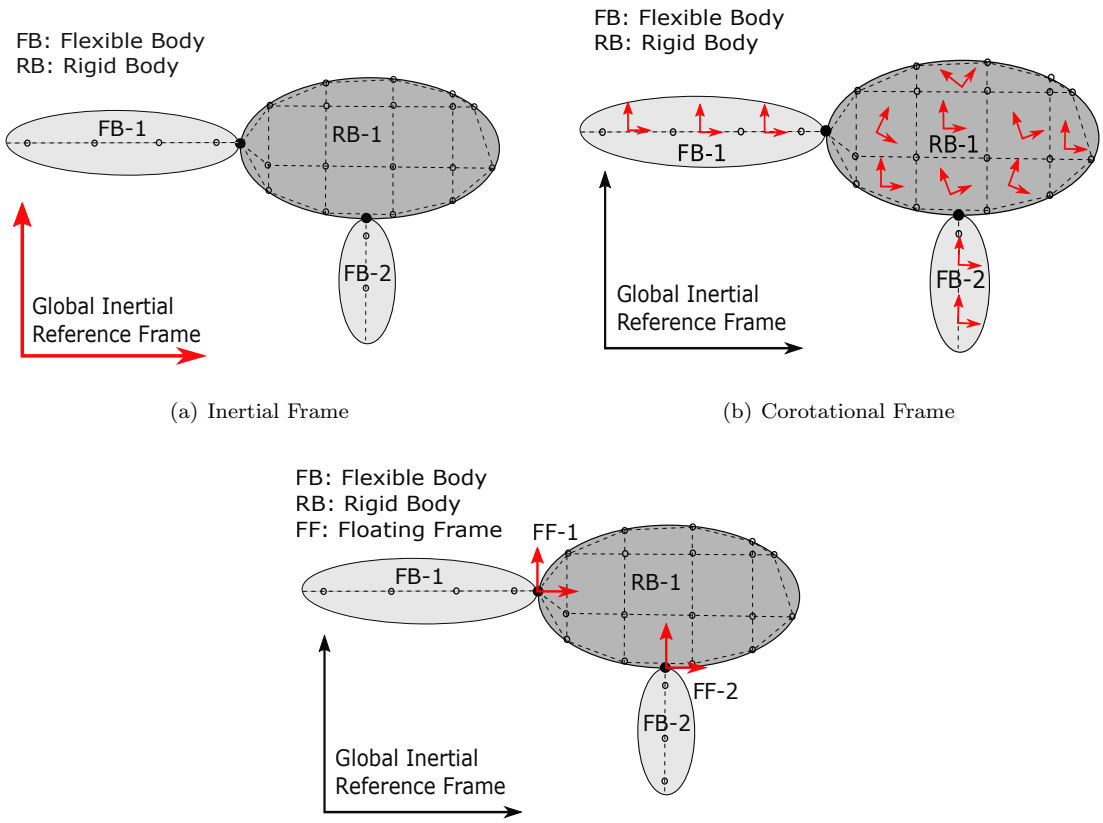

(a) Inertial Frame

(b) Corotational Frame

(c) Floating Frame

Figure 2. Common multibody frame formulations

the elements are superimposed using linear FEM mass and stiffness matrices. The formulation still captures the non-linear elastic deformation within an element, because each discretised element has its own reference frame, as visualised in Fig. 2(b). Lastly, the *floating frame formulation* is an extension of rigid multibody dynamics to a flexible multibody system. In this method, small elastic deformations are superimposed on large rigid body motion to represent the motion of floating frame, which moves along with the body. The floating frame is typically placed at the interface between two bodies (although it can be placed anywhere on the body), as shown in Fig. 2(c). The elastic deformations are obtained from mode shapes and eigenfrequencies, which are either computed numerically or experimentally for each flexible link. A detailed comparative study of the three formulations can be found in Ref. 3.

Based on the requirements from the model, the three formulations can be analysed. In terms of achieving good accuracy within feasible computation time, the *floating frame formulation* has an advantage. According to Ref. 3, the formulation allows modal reduction, which reduces the computation time without much loss in accuracy. With the other two formulations, it is possible to get accurate results but only at the expense of additional computation time. The *co-rotational formulation* cannot differentiate between rigid and flexible elements. The rigid bodies are modelled as stiffer flexible elements, which results in an inefficient model for the application (due to the large computation time). Also, the *inertial frame formulation* tends to suffer from frame invariance, which is an apparent lack of variation in some physical quantities (like material properties and mass), due to interpolation of large rotations.

When it comes to constraint handling, the joints in *inertial frame formulation* and *co-rotational frame formulation* can be simply constrained by overlapping nodes. The constraints for *floating frames formulation* is usually done through Lagrange multipliers, which is not so straight forward. Additionally, the Lagrange multipliers add more unknowns to the system EOM, which increases the computation time. This disadvantage can be overcome by defining the motion of the floating frame in terms of absolute interface coordinates

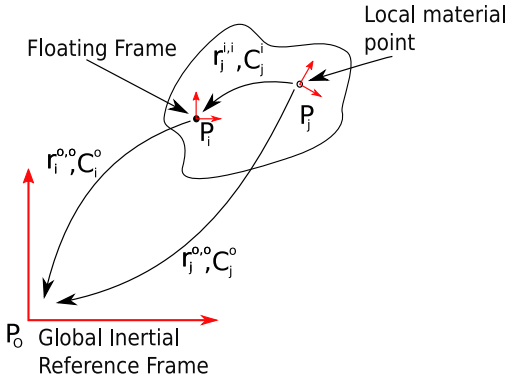

Figure 3. Position of material points P_j with respect to inertial frame at point P_o using floating frame at point P_i

as proposed in Ref. 1. The term absolute interface coordinates refers to the generalised coordinates of the interface points located at the joints between any two bodies in the FMS, defined with respect to the inertial frame. By doing this (provided there is no deformation at the location of floating frame), the constraints can be applied directly by overlapping nodes and the Lagrange multipliers are no longer required.

The *inertial frame formulation* and *co-rotational frame formulation* are beneficial when large elastic deformations are involved. However, the test case in hand will have relatively small elastic deformations as space structures typically do not undergo large deformations.[3] Lastly, *floating frame formulation* is an extension of rigid multibody dynamics, which facilitates easy comparison of the rigid and flexible models. From the above discussion, it can be concluded that floating frame is a good fit for the research. The possibility of using model-order reduction techniques and the constraint handling from the new method, makes this formulation an attractive choice for control simulation. It must be stated, however, that the formulation is relatively more complex than the other two. The process of deriving EOM for the system based on the new method will be discussed in further detail in the coming section.

B. Generalised Equations of Motion

Having discussed the different aspects involved in the floating frame formulation, the kinematic and dynamic EOM can be derived. The dynamic equations need to be reduced using an established model reduction method (Craig-Bampton reduction). Further, to write the EOM in terms of absolute coordinates of interface points, a transformation needs to be performed from the floating frame to these coordinates. To achieve this, the EOM are first derived with respect to the floating frame and converted to absolute coordinates using transformation matrices. In this section, the steps to achieve the final EOM will be summarised. The detailed derivation of the equations can be found in Ref. 1.

Before defining the kinematics of a multi-body system consisting of both rigid and flexible elements, it is foremost to define the kinematics of a material point, P_j, on a flexible body with respect to the floating frame reference (FFR) located at point, P_i, as shown in Fig. 3. The absolute position of the FFR is defined with respect to the inertial frame (with origin at P_o) using the position vector, $\boldsymbol{r_i^{o,o}}$ and the rotation (or transformation) matrix, $\boldsymbol{C_i^o}$. Note that the notation superscript "A,B" on the position or velocity vectors (e.g., $\boldsymbol{r_i^{A,B}}$) indicates the position of point "P_i" defined in frame A, relative to the frame at B. Also, for the rotation matrix, the subscript A and superscript B indicates a transformation from frame A to frame B. Similarly, the position of material point P_j is defined with respect to the floating frame P_i using the position vector, $\boldsymbol{r_j^{i,i}}$ and the rotation matrix, $\boldsymbol{C_j^i}$. This results in an expression for relative velocity of P_j with respect to P_i, which is given by the difference between the absolute velocities of the material point and the FFR. This is given by:

$$\boldsymbol{v_j^{i,i}} = \left[\boldsymbol{C_o^i}\right]\boldsymbol{v_j^{o,o}} - \left[-\tilde{\boldsymbol{r}}_{\boldsymbol{j}}^{\boldsymbol{i,i}}\right]\left[\boldsymbol{C_o^i}\right]\boldsymbol{v_i^{o,o}} \tag{1}$$

Here, the "[ ]" will be used as a simplified notation for the compound matrices. $\boldsymbol{v_j^{o,o}}$ and $\boldsymbol{v_j^{i,i}}$ are $(6N \times 1)$ vectors containing all variations of the absolute and local interface coordinates with time, respectively. Here, N is the number of interface points. $\left[\boldsymbol{C_o^i}\right]$ is a $(6N \times 6N)$ block diagonal matrix consisting of all rotation matrices associated with the respective interface points. Lastly, $\left[-\tilde{\boldsymbol{r}}_{\boldsymbol{j}}^{\boldsymbol{i,i}}\right]$ is the column-assembly of all (6×6) skew-symmetric matrices representing displacement and rotation of all interface points, when the system

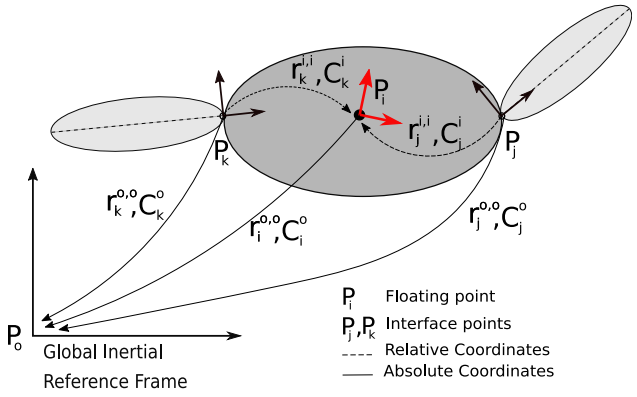

Figure 4. Relative and absolute representation of interface points, P_j and P_k

experiences rigid body motion in a certain direction with respect to the FFR.

Next, a relation needs to be defined between the local elastic velocities and absolute velocities of the material point or interface point. Assuming that the elastic deformation of the flexible elements is small, the flexible body can be discretised into many linear finite elements called superelements. These superelements can be used to define the dynamics with respect to a floating frame at P_i with a constant mass matrix $\boldsymbol{M_i}$ and stiffness matrix $\boldsymbol{K_i}$. This can be achieved by establishing generalised coordinates, $\boldsymbol{q^{j,j}}$, to represent the deformation using the modes obtained after model reduction using the Craig-Bampton (CB) method (detailed description in Ref. 4). This is applicable under the assumption that the deformation can be represented by a linear combination of selected modes.[1] The deformation will include the small elastic displacements, $\boldsymbol{u_j^{i,i}}$, and rotation of the interface points, $\boldsymbol{\theta_j^{i,i}}$. Therefore, the generalised coordinates can be written as:

$$\boldsymbol{q_j^{i,i}} = \begin{pmatrix} \boldsymbol{u_j^{i,i}} \\ \boldsymbol{\theta_j^{i,i}} \end{pmatrix} \tag{2}$$

Since rotations cannot be expressed as proper vectors, the orientation after deformation cannot be simply expressed as the sum of the undeformed orientation and elastic rotation. Therefore, it is assumed that the undeformed orientation of a material point with respect to the local frame is always zero, i.e., the undeformed local rotation matrix becomes an identity matrix. So, the final local orientation of a material point after deformation can be described as change in the rotation of the interface point $\boldsymbol{\theta_j^{i,i}}$. This results in an expression for the local elastic velocity ($\boldsymbol{\dot{q}_j^{i,i}}$) with respect to FFR in terms of generalised coordinates of the interface point. It is given by the difference between the absolute velocity of the interface points (containing both elastic and rigid body modes) and the rigid body motion of the body in terms of absolute velocity of FFR as shown below:

$$\boldsymbol{\dot{q}_j^{i,i}} = [\boldsymbol{C_o^i}]\boldsymbol{v_j^{o,o}} - [-\boldsymbol{\tilde{r}_j^{i,i}}][\boldsymbol{C_o^i}]\boldsymbol{v_i^{o,o}} \tag{3}$$

However, since the FFR and the elastic modes both account for rigid body motion, there is an overlap. The extra rigid body modes are eliminated by computing the CB modes at the location of FFR, placed at the body's centre of mass. It is assumed that the center of mass remains the same in both deformed and undeformed configuration. This constraint is represented by:

$$[\boldsymbol{\phi_{CB}^i}]\boldsymbol{\dot{q}_i^{i,i}} = \boldsymbol{0} \tag{4}$$

where $[\boldsymbol{\phi_{CB}^i}]$ is the $(6 \times 6N)$ matrix of CB modes evaluated at the FFR. This ensures that the rigid body modes are represented by the FFR and only the elastic modes are taken into account from the CB reduction, thereby eliminating the non-unique modes. Note that due to the non-linear relation between relative and absolute position of the interface points, as well as the floating frame (because the system changes with time), these constraints cannot be solved at position level

To be able to model the dynamics in terms of absolute interface coordinates, and also, to apply constraints without the use of Lagrange multipliers, the floating frame can now be removed from the kinematic description using transformation matrices.

Figure 4 shows a body with the floating frame located at P_i on the rigid hub, connected to two flexible appendages. The interface points P_j and P_k are placed at the connection points of these bodies, with their position defined with respect to the floating frame using generalised coordinates (with reduced degree of freedom), $\boldsymbol{q_j^{i,i}}$ and $\boldsymbol{q_k^{i,i}}$. The floating frame itself is defined with respect to the inertial frame with $\{\boldsymbol{r_i^{o,o}}, \boldsymbol{C_i^o}\}$. By eliminating the floating frame, the position of the interface coordinates is given by $\{\boldsymbol{r_j^{o,o}}, \boldsymbol{C_j^o}\}$ and $\{\boldsymbol{r_k^{o,o}}, \boldsymbol{C_k^o}\}$. Using similar notations for N interface points, the transformation matrices (derived in detail in Ref. 1) can be written as:

$$[\boldsymbol{Z^i}] = [\boldsymbol{Q^i}]^{-1}[\boldsymbol{\phi_{CB}^i}] = [\boldsymbol{Q^i}]^{-1}\begin{pmatrix}\phi^1 & \cdots & \phi^N\end{pmatrix} \tag{5}$$

and

$$[\boldsymbol{T^i}] = \boldsymbol{I} - [\boldsymbol{\phi_{rig}^i}][\boldsymbol{Z^i}] \tag{6}$$

where $[\boldsymbol{Q^i}]$ is a (6×6) matrix representing the elastic deformation of the interface points and $[\boldsymbol{\phi_{rig}^i}]$ is a $6N \times 6N$ compound matrix containing the rigid body modes for all interface points. $[\boldsymbol{Z^i}]$ is a $(6 \times 6N)$ transformation matrix, which defines the relation between the absolute motion of the interface coordinates and the absolute motion of the floating frame. It can be physically represented as the rigid body motion due to the motion of an interface point on floating frame at P_i. Lastly, $[\boldsymbol{T^i}]$ is a $(6N \times 6N)$ transformation matrix which defines the relation between the absolute and local motion of the interface coordinates. It can be physically interpreted to remove the rigid body motion from the motion of an interface point, such that only the velocity of the elastic part remains.[5] The final velocity equation in terms of the transformation matrices is given by:

$$\begin{pmatrix}\dot{\boldsymbol{q}}_i^{o,o} \\ \dot{\boldsymbol{q}}^{i,i}\end{pmatrix} = \boldsymbol{A}\dot{\boldsymbol{q}}^{o,o}, \qquad \text{where} \qquad \boldsymbol{A} = \begin{bmatrix}[\boldsymbol{C_i^o}][\boldsymbol{Z^i}][\bar{\boldsymbol{C}}_o^i] \\ [\boldsymbol{T^i}][\bar{\boldsymbol{C}}_o^i]\end{bmatrix} \tag{7}$$

where $\dot{\boldsymbol{q}}^{i,i}$ represents a $6N \times 1$ column matrix containing the local velocities relative to the floating frame due to elastic deformation in the body. Therefore, Eq. (7) allows the successful formulation of the dynamic equations of floating frame completely in terms of inertial coordinates.

Finally, the equations of motion can be derived based on the Principle of Virtual Work (see Ref. 6 for details). Therefore, the generalised equation of motion for a FMS can be written in the form:

$$\boldsymbol{M\ddot{q} + C\dot{q} + Kq = F} \tag{8}$$

Here, the $\boldsymbol{M}$ and $\boldsymbol{K}$ denote the global mass and stiffness matrices, $\boldsymbol{q}$ are the generalised coordinates of the floating frame and local frames of the system, $\boldsymbol{C\dot{q}}$ includes the quadratic velocity inertia forces due to terms like damping, centrifugal and Coriolis forces, and lastly, $\boldsymbol{F}$ includes the externally applied forces and moments like gravity gradient, control torques and so on. In a more expanded floating frame formulation, the equation can be written as:

$$\begin{bmatrix}\boldsymbol{M_{rr}^i} & \boldsymbol{M_{rf}^i} \\ \boldsymbol{M_{f,r}^i} & \boldsymbol{M_{ff}^i}\end{bmatrix}\begin{pmatrix}\ddot{\boldsymbol{q}}_i^{o,o} \\ \ddot{\boldsymbol{q}}_j^{i,i}\end{pmatrix} + \begin{bmatrix}\boldsymbol{C_{rr}^i} & \boldsymbol{C_{rf}^i} \\ \boldsymbol{C_{f,r}^i} & \boldsymbol{C_{ff}^i}\end{bmatrix}\begin{pmatrix}\dot{\boldsymbol{q}}_i^{o,o} \\ \dot{\boldsymbol{q}}_j^{i,i}\end{pmatrix} + \begin{bmatrix}\boldsymbol{0} & \boldsymbol{0} \\ \boldsymbol{0} & \boldsymbol{K_{ff}^i}\end{bmatrix}\begin{pmatrix}\boldsymbol{0} \\ \boldsymbol{q_j^{i,i}}\end{pmatrix} = \begin{pmatrix}\sum \boldsymbol{F_i^o} \\ \boldsymbol{L_j^i}\end{pmatrix} \tag{9}$$

In the above equation, the subscript f indicates the flexible part and r indicates the rigid part. A coupling between rigid and flexible DOF is indicated by rf or fr. Also, it can be noted that the stiffness matrix only has a flexible part, because the rigid body does not induce any elastic forces. Vector $\sum \boldsymbol{F_i^o}$ is the sum of all external forces and moments in the floating frame with respect to the inertial frame. $\boldsymbol{L_j^i}$ gives the effect of an external force or moment on the mode shapes. Performing the transformation in Eq. (8) using Eq. (7), the equations of motion become:

$$\boldsymbol{A^T M A\ddot{q}^{o,o} + A^T(M\dot{A} + CA)\dot{q}^{o,o} + A^T K q^{i,i} = A^T F} \tag{10}$$

By making some simplifying assumptions, the equations can be reduced to:

$$[\bar{\boldsymbol{R}}_j^o][\boldsymbol{M_{CB}}][\bar{\boldsymbol{R}}_o^j]\ddot{\boldsymbol{q}}^{o,o} + [\bar{\boldsymbol{R}}_j^o][\boldsymbol{T_i}]^T[\boldsymbol{C_{loc}}]\dot{\boldsymbol{q}}^{o,o} + [\bar{\boldsymbol{R}}_j^o][\boldsymbol{T_i}]^T[\boldsymbol{K_{CB}}]\boldsymbol{q}^{i,i} = \boldsymbol{F^o} \tag{11}$$

where $[\boldsymbol{M_{CB}}]$ and $[\boldsymbol{K_{CB}}]$ represent the local mass and stiffness matrices obtained from the FE model after performing CB reduction. While $[\boldsymbol{C_{loc}}]$ is the generalised velocity matrix (detailed description in Ref. 7). It can be noticed that the elastic forces are still expressed in terms of floating frames and not with respect to inertial frame. This is because the transformation to absolute coordinates cannot occur at position level. Comparing the terms of Eqs. (10) and (11), the stiffness matrices in both the equations are the same. To match the acceleration and velocity terms, it is assumed that,[8]

1. The mass matrices are expressed in the undeformed configuration of the component (for the acceleration term).

2. The mass matrix is lumped (for the velocity term).

3. Each body is defined by one element at the interface points, which guarantees that the interface points chosen for this formulation and the floating frame formulation are the same (for velocity term).

Additionally, test cases simulated in Ref. 1 prove that neglecting the quadratic inertia terms, do not have a significant impact on the simulation accuracy for small deformation cases. Therefore, for the current simulation, these forces will not be considered. A more detailed derivation of these assumptions can be found in Ref. 8. Therefore, Eq. (11) represents the final EOM of a superelement, suitable for the simulation of flexible multibody dynamics.

C. Verification and Validation

A software was developed based on the process stated in the previous section. Figure A1 shows the basic architecture of the simulator. In the figure, the blocks highlighted in blue represent the structural dynamics of a flexible system, which acts as a plant for the control system. The multibody model consists of four blocks, for initialisation, body level calculations, multibody level calculations and solution of equations of motion. In this section, the working of the plant model will be validated using test cases given in Ref. 1, originally adapted from Ref. 9 (slider crank) and Ref. 10 (spherical jointed beam). Additionally, the kinetic energy, elastic energy, total energy and internal/external work of the system will be examined to understand the dynamics better and to ensure that the total energy is balanced.

By law of conservation of energy, the total energy, E_{tot}, of the system (assuming no dissipation) should be conserved at every time step. This should account for elastic energy (or potential energy), E_{elas}, kinetic energy, E_{kin}, and external work of the system, W_{ext}. Therefore, the total energy of the system is calculated using

$$E_{tot}(t) = E_{elas}(t) + E_{kin}(t) + W_{ext}(t) \tag{12}$$

Further, the elastic energy should be calculated for each element at the body level[7] at each time step. It is given by:

$$E^b_{elas}(t) = \frac{1}{2}\left(\boldsymbol{u^{i,i}}(t)\right)^T \boldsymbol{K_{CB}}\left(\boldsymbol{u^{i,i}}(t)\right) \tag{13}$$

where, $\boldsymbol{u^{i,i}(t)}$ is the elastic deformation of each element with respect to the floating frame at time t. Then, the total elastic energy is calculated at the multibody level (for N bodies) given by:

$$E_{elas}(t) = \sum_{b=1}^{N} E^b_{elas}(t) \tag{14}$$

The kinetic energy is also calculated at multibody level and is given by:

$$E_{kin}(t) = \frac{1}{2}\left(\boldsymbol{v^{o,o}}(t)\right)^T \boldsymbol{M_{sys}} \boldsymbol{v^{o,o}}(t) \tag{15}$$

where $\boldsymbol{v^{o,o}}(t)$ is the velocity of each element with respect to the inertial frame at time t. $\boldsymbol{M_{sys}}$ represents the total mass of the system. The total work is calculated as the sum of initial energy of the system and the work done by external forces $W(t)$, integrated over the total time, T, as shown below:

$$W(t) = \int_{t=0}^{T} \mathrm{d}W(t)\ \mathrm{d}t + E_{init} = \int_{t=0}^{T} (F^o(t))^T \boldsymbol{v^{o,o}}(t)\ \mathrm{d}t + E_{init} \tag{16}$$

where $\boldsymbol{v^{o,o}}(t)$ is the velocity vector of the interface point with respect to inertial frame and $F^o(t)$ represents the external forces acting at the interface. Lastly, E_{init} represents the initial energy of the system, which comes from the prescribed motion to the system. For the validation, the first test cases is that of a 2D slider crank mechanism.[9] The configuration of the system is shown in Fig. 5(a). The system consists of a rigid crank, which is rotating with a constant prescribed angular velocity of 150 rad/s. The crank is then attached to a flexible connector of length 0.3 mm and a circular cross-sectional radius of 0.006 m. The

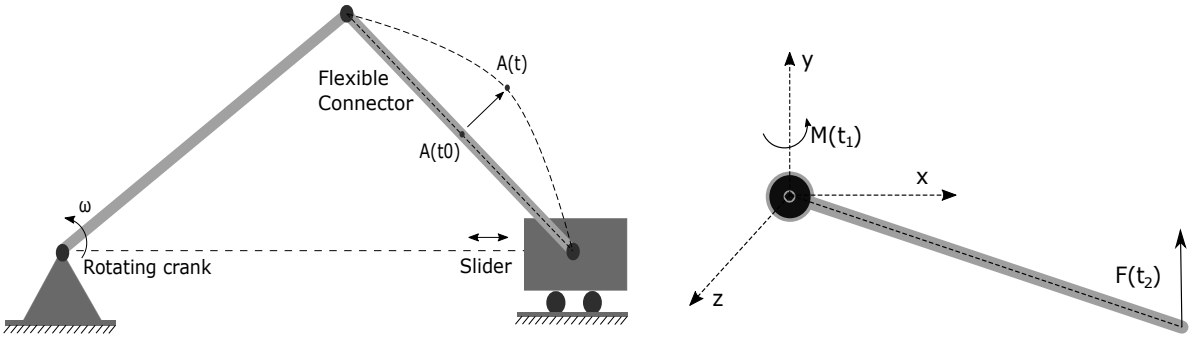

(a) Slider Crank (b) Beam with spherical joint

Figure 5. Test case for validation

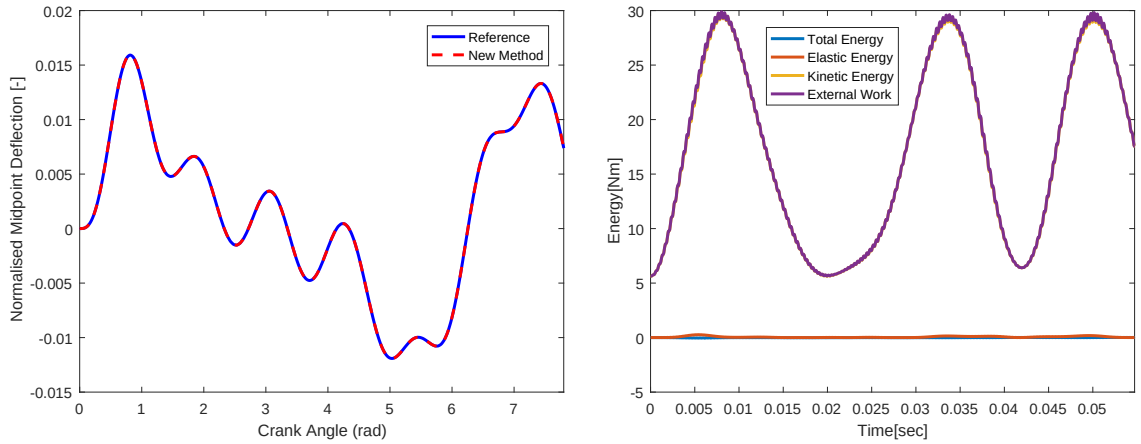

(a) System response (b) Energy balance

Figure 6. Test Case 1: Slider Crank

connector is assumed to have material properties of steel, i.e., a Young's modulus of $2{\cdot}10^{11}$ N/m^2 and mass density of 7800 kg/m^3. The other end of the connector is then linked to a slider, which is allowed to move without friction. The mass of the slider is half of that of the connector. The constant angular velocity prescribed to the crank should induce a linear motion in the slider in the absence of flexibility. However, due to the elastic deformation of the connector, some perturbations can be observed in the slider motion. To model the dynamics of flexible connecter, it is divided into three nodes. The point A in Fig. 5(a), which is halfway between the two end points serves as the location for floating frame. The other two end points act as interface points. Figure 9 shows the displacement or mean motion of the midpoint throughout the simulation. On comparing with the reference dynamics obtained from the multibody software "Spacar", the results from the new method show an exact match. Figure 6(b) shows the the total energy of the system. It can be seen that the work done by the system is translated into kinetic energy and the total energy of the system remains zero and hence, conserved.

The second test case is that of a 3D beam constrained by a spherical joint at one end,[10] as shown in Fig. 5(b). The beam is 141.42 mm long with a cross-section area of 9 mm^2 and an area moment of inertia of 6.75 mm^4. The mass density is $7.8{\cdot}10^{-3}$ kg/mm^{-3} and a Young's Modulus of $2.1{\cdot}10^6$ N/mm^2. The beam is given a torque of 200 Nmm about the vertical axis for the first 10.2 s and then, an impulsive force of 100 N is applied at the tip in the vertical direction. The beam is modelled using two beam elements, and the resulting motion is completely in response to the external force and moment. The absolute angular velocity about the vertical axis is plotted against time. From Fig. 7(a), it can be seen that the new method matches the reference very closely. Further, in Fig. 7(b), a clear rise in the system's energy can be seen when the impulse is added to the system. The energy remains conserved at all time as the sum of the system's kinetic energy, elastic energy and external work. Both cases follow the law of conservation of energy, thus verifying

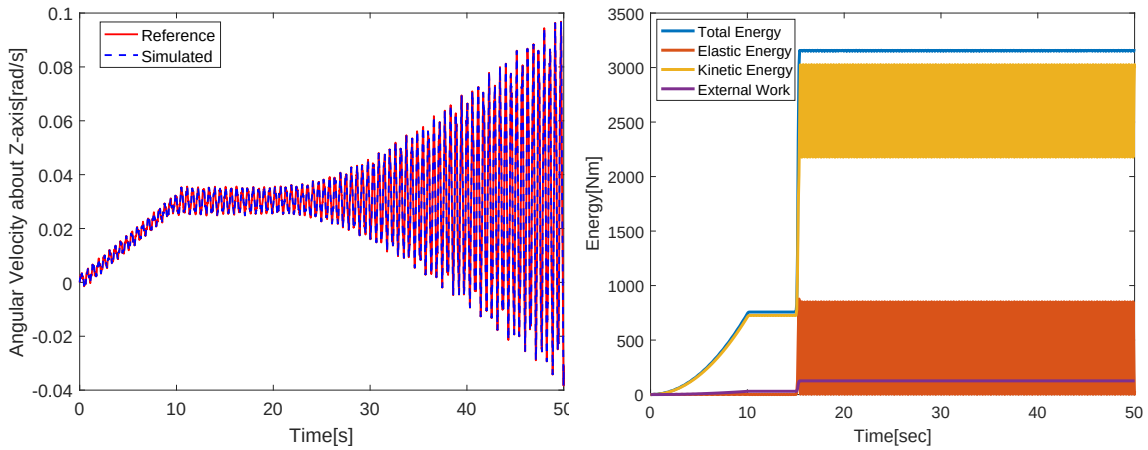

(a) System response (b) Energy balance

Figure 7. Test Case 2: Beam with Spherical Joint

the software based on the new formulation. The structural model of the satellite can be modelled to fit the software design.

III. Satellite Structural Model

To model the dynamics and control for the different phases of the e.deorbit mission, the geometry and mass properties of the required configurations must be discussed. In the synchronisation phase, wherein the chaser synchronises with the target attitude, the geometric and mass properties of the chaser are required to model the FMD and also, to determine the control moments. Also, the geometric and mass properties of the target needs to be summarised to derive the combined chaser-target properties in the stacked configuration, at which point it is assumed that the chaser has successfully docked with the target and achieved a rigid contact. Therefore, the required attributes of the configuration will be introduced in Sec. III.A.

A typical multibody structure can be divided into flexible and rigid bodies. The displacement field consists of the flexible elastic deformation superimposed on the rigid body motion. To define the position of the floating frame in the deformed configuration with respect to the interface points, it is advantageous to select a beam or plate configuration. This is because the deformation of any material point on these elements can be easily defined with respect to the local frame using established shape functions. Therefore, in this research, the flexible appendages will be represented using beam elements. The number of beam elements, material properties and mass properties also play a crucial role in defining the flexible dynamics accurately. A sensitivity study will be performed for selection of these parameters for both e.deorbit and stacked configurations in Sec. III.B.

Since the elastic vibrations are perturbations to the rigid body motion, the commands to the controller are based on the rigid body dynamics of the system (as can be seen from Fig. A1). Also, the control moment is applied to the centre of mass of the configuration, which lies on the rigid hub due to its large mass. Therefore, it is crucial to also incorporate the rigid body dynamics in the flexible multibody system. In other words, the controller design for the flexible multibody system (minus the elastic perturbations) should be based on the same (satellite) properties as the rigid body. This also facilitates the comparative study of control-structure interaction of the flexible model as compared to the rigid model. The adaptation of rigid inertia properties to the flexible system will be discussed in Sec. III.C

A. System configuration

The initial launch mass of Envisat was 8138 kg with 319 kg of hydrazine. According to Ref. 11, the current mass of Envisat is 7828 kg, which means it is assumed that all the propellant is consumed. The spacecraft body consists of a rigid hub of dimensions 10×2.8×2.6 m and three major flexible appendages - the large solar array, the SAR antenna and a Ka-dish band.[12] For simplicity, in this research, only the flexibility due

to the presence of the solar panel will be considered. The solar panel, which is 14.2 m long and 5 m wide, weighs 338 kg. It is assumed that the axis of the solar panel is aligned with that of the rigid hub. According to ESA, the total mass moment of inertia of the target including the solar panel about its principle axis is:

$$\boldsymbol{J_{tar}} = \begin{bmatrix} 16969 & 0 & 0 \\ 0 & 124700 & 0 \\ 0 & 0 & 129077 \end{bmatrix} \text{ kg m}^2 \tag{17}$$

According to Ref. 12, the launch mass for the Chaser is 1628 kg, with 762 kg of dry mass and 826 kg of consumables. The estimated final mass on achieving orbit in the vicinity of Envisat is around 1480 kg.[13] It is assumed that the shape of the chaser is a rectangular box of dimensions 1.2×1.2×3 m. It has a solar panel of dimensions 2.9×1.1×0.05 m and mass 25 kg, placed at 3.5 m from the centre of mass of the chaser. The centre of mass is assumed to be the geometric centre of chaser's box shaped body. The mass moment of inertia based on these dimensions, is given by:[13]

$$\boldsymbol{J_{cha}} = \begin{bmatrix} 1521 & 0 & 0 \\ 0 & 1322 & 0 \\ 0 & 0 & 560 \end{bmatrix} \text{ kg m}^2 \tag{18}$$

Lastly, assuming that the chaser docks with Envisat in the configuration shown in Fig. 1, the properties can be calculated. The total mass of the stacked system, M_{stack} is simply the sum of mass of Envisat, M_{tar} and mass of chaser, M_{cha}:

$$M_{stack} = M_{tar} + M_{cha} = 7828 + 1480 = 9308 \text{ kg} \tag{19}$$

The combined mass of flexible elements is taken as the sum of mass of both solar panels, which is equal to 413 kg. For simplicity, it is assumed that both solar panels have the same material properties (like Young's modulus). Lastly, the total rigid body inertia of the stacked configuration about the principle axis is given by:[13]

$$\boldsymbol{J_{stack}} = \begin{bmatrix} 130521 & 0 & 0 \\ 0 & 27282 & 0 \\ 0 & 0 & 134251 \end{bmatrix} \text{ kg m}^2 \tag{20}$$

Based on these properties, both the rigid and flexible bodies of the multibody system will be modelled.

B. Modelling of flexible elements

As stated before, the flexible panels in both the synchronisation and stacked configurations will be modelled as beams. Therefore, to model the dynamics of the solar panels as closely as possible using beams, a number of parameters must be carefully selected. These are:

- *Young's Modulus (E)*: This is a property of a material to resist deformation along an axis in the presence of forces. The higher the value of Young's modulus, the stiffer is the material. According to Ref. 14 and Ref. 15 a 1 m long solar panel, the Young's modulus ranges between 4.8×10^{10} N/m^2 to 5.8×10^{10}N/m^2. For this research, it will be assumed that a 1 m long beam element representing a solar panel has E=5.8×10^{10} N/m^2.

- *Poisson's ratio*: It is assumed that the elastic deformations are small and there is no strain (or yield) in the system. Therefore, a Poisson's ratio of 0.3 taken.

- *Length*: The length of a beam element also has an effect on stiffness. The smaller the beam element, the higher will be its stiffness (for the same cross-sectional area and Young's modulus). However, the total length of the solar panel (or sum of beam elements) is taken equal to the length of the solar panel.

- *Cross-section area*: Modelling of beams demand that the cross-sectional area of the beam is negligible compared to the length. Therefore, rectangular cross-section dimensions of 0.03×0.03 m are assumed.

- *Discretisation of beam elements*: The term discretisation refers to the number of beam elements the flexible body is divided into. For the same Young's modulus and cross-sectional area, the larger the

Table 1. Material properties of chaser solar panel (sensitivity analysis)

	No. of beam elements [-]	Young's Modulus [Nm^{-2}]	Length per element [m]	Mean computation time [s] (10 runs)
Case 1	1	1.71×10^{11}	2.90	993
Case 2	3	5.64×10^{10}	0.97	6717
Case 3	5	3.50×10^{10}	0.58	11131

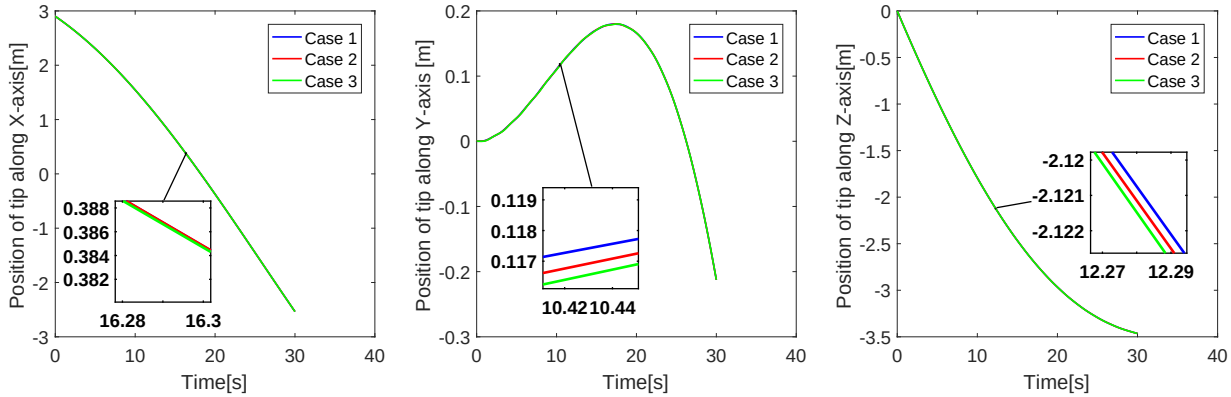

Figure 8. Position of tip of solar panel about X, Y and Z axis for 3 cases given in Table 1

discretisation, the smaller will be the length of the beam element. This results in a stiffer system. For very long flexible bodies, discretisation is required, because the Young's modulus cannot be made too high to attain stiffness. However, for dynamic analysis, the number of interface points increase and the state vector becomes very large. This results in large computation time. Therefore, it is imperative to find a balance between length, Young's modulus and discretisation to model the flexible elements as accurately, without much increase in the computation time.

- *Density*: The density of the flexible elements is computed by dividing the mass of the solar panel by the volume of the beam. This is done to capture the mass properties of the solar panel, which has a crucial role in the flexible dynamics.

- *Boundary Conditions*: In this research, it is assumed that the chaser is already at the location of Envisat and needs to synchronise with its attitude at a fixed location. In other words, it is assumed that there is no translational motion and the satellite must spin about its centre of mass at the same location. Therefore, assuming the rigid body as a point mass, the solar panel is constrained on one end with a spherical joint. This allows the solar panel to have an angular velocity in any direction, but constrains the position of the end attached to the rigid body. In the stacked configuration, a similar assumption is made. The rigid body is assumed to point acting like a rigid hinge between the two panels, allowing rotation about this fixed point, but constraining the position of the ends attached to the rigid body.

To find the correct balance between length (L), Young's modulus (E) and discretisation (number of beam elements), a sensitivity study will be performed to get the best performance in terms of accuracy and computation time. Theoretically, by maintaining the same E/L ratio, it should be possible to have the same elemental stiffness. For the chaser solar panel length of 2.9 m, this analysis will be performed for three test cases as shown in Table 1. For different number of beam elements, the same E/L ratio is maintained. The absolute position of the tip node is studied to analyse the effect on accuracy, for a constant angular velocity of 2 °/sec about all axis for 30 s simulation time and timestep of 10^{-3} s. The computation time is also studied over 10 runs each for the three cases. Figure 8 shows that the effect of discretisation on the accuracy is not large, since all three axes show very comparable results. However, the simulation time tabulated in Table 1 shows that Case 1 has the least computation time. Therefore, for the rest of the research, flexible elements will be modelled using the material properties stated for Case 1. For consistency, the same length

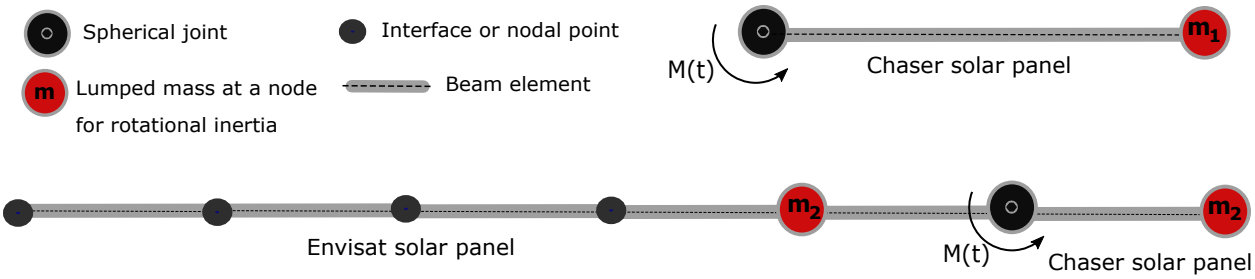

Figure 9. Simplified representation of the structural model for synchronisation (top) and connected (bottom) phases.

of beam elements will be used to define the solar panels of stacked configuration as well. This will require the target solar panel, which is 14.2 m long, to be divided into five beam elements.

C. Modelling of rigid elements

An important property of a rigid body that plays a major role in the dynamics of a system is the mass moment of inertia (also called rotational inertia). It is a measure of body's resistance to change its direction of rotation and magnitude. Since it depends on the mass and dimensions of a body, the stacked configuration has an inherently larger rotational resistance. However, according to Ref. 16, rotary inertia can be added to a flexible system using lumped masses. But, lumped masses are point masses, which do not have a geometry and, therefore, cannot have an inertia about their own axis. This eliminates the possibility to place the lumped mass at the spherical joint in the flexible model (where the control moment is also applied). Therefore, to add rotational inertia to the rigid body the lumped masses are placed at the adjacent node (or the next interface point). This way, the inertia can be translated to the constrained node using Steiner's parallel axis theorem, which gives a relation between the inertia matrix of a body with mass, M, relative to the centre of mass (I_{COM}) and the inertia matrix relative to another point O (I_O) at a distance, d, from the centre of mass of the body. This gives:

$$I_O = I_{COM} + Md^2 \tag{21}$$

For a point mass, the inertia simply becomes Md^2. Note that the mass matrix used here is a diagonal matrix. It should also be noted that the flexible body itself has some rotational inertia. For a slender beam, the inertia can be computed about an axis at an end point using $I = mL^2/3$, where m is the mass and L is the length of the beam. It must be noted that for a slender beam, the inertia about the axis along the length is negligible, while the other two axes can be computed using mL^2. The sum of the inertia from the lumped masses, $\boldsymbol{I_m}$, and, that from the slender beam, $\boldsymbol{I_s}$ should account for the total inertia of the system, $\boldsymbol{I_T}$, which is given by Eq. (18) for the chaser and Eq. (20) for the stacked configuration. Therefore, the lumped mass can be calculated about each axis using:

$$I_T = I_s + Md^2 \tag{22}$$

$$M = (I_T - I_s)/d^2 \tag{23}$$

It must be stated that the computation of mass moment of inertia for flexible body is not the perfect representation of the body's inertia. This may lead to a small mismatch in the inertia of the flexible multibody system and the rigid body inertia stated in Sec. III.A. The inaccuracies in the model can be detected by using a controller based on inverse dynamics, which is dependent on the system inertia. Any mismatch in the inertia modelling would lead to a steady state error in the response of the system once it is stabilised. It is possible to model the inertia better using shape integrals defined with respect to the global frame (see Ref. 16 for details). However, for this research, this method is not implemented.

Figure 9 shows the simple representation of the final configuration of the system of the chaser and the stacked model for synchronisation and connected phases respectively. Note that the lumped masses (shown in red) are added to the fixed mass matrices of the interface point (or node) only after the CB reduction has been performed. This ensures that only the natural modes are not affected by the "pseudo" modelling of the rigid body inertia. To perform a preliminary analysis of the expected dynamics based on the different phases of the mission, it can be stated that:

- *Synchronisation:* The chaser configuration needs to start from zero angular velocity and match the target attitude, including angular velocity and orientation (which is also constantly changing with time). Sudden control moments applied at the spherical joint shown in Fig. 9 will cause vibration in solar panel, which will further cause a disturbance in angular velocity. Since the inertia of the chaser and also the size (and mass) of the flexible element is smaller, it must be relatively easier to control the satellite in the presence of elastic perturbations.

- *Connected:* From the figure, it can also be observed that the stacked configuration has large asymmetry in geometry as well as large inertia. Since it is tumbling at a rate of 3.5 °/s about all axes, the system becomes very dynamic (with possibly very large vibrations) and difficult to control.

Hence, the controller design to control such a dynamic multibody system will be discussed in the next section.

IV. Control System Design

Attitude control of satellites with large, flexible appendages can become complicated in the presence of oscillations induced due to (sudden) attitude changes. The stacked configuration of a chaser spacecraft with a large, passive target aggravates the control design even more, considering the asymmetry in both mass properties and geometry. The classical PD (Proportional and Derivative) controller, which is still widely used in spacecraft attitude control, may not be robust enough to handle all abrupt manoeuvres required. Further, if the control input is not smooth, it may result in adding to the vibration of the solar panels. Robust control algorithms that can counteract the uncertain nonlinear dynamics is a possible way to guarantee the stability of the satellite. One such control system that is based on the dynamics of the system is Nonlinear Dynamic Inversion (NDI). The NDI controller enables multivariable control and avoids gain-scheduling by directly incorporating the nonlinear dynamics in the control law. However, NDI is very sensitive to model mismatches and measurement errors, which can result in instability. Therefore, a new variation of NDI called Incremental Nonlinear Dynamic Inversion (INDI) was developed to retain the advantages and to reduce vehicle model dependency of NDI.[17] This controller with its increased robustness may become a good fit for attitude control in the presence of elastic disturbances.

In this chapter, the guidance and control part of the simulator design shown in orange and green in Fig A1 will be explained. First the selection of attitude parameterisation and other control parameters required for the control system design will be discussed in Sec. IV.A. Since guidance is based on the rigid body dynamics, the basic EOM used will also be stated. Then, the control theory for the two controllers will be summarised in Sec. IV.B.

A. Guidance

As stated before, it is assumed that the rotational motion is decoupled from the translational motion, *i.e.,* the orbital position is frozen. Since the guidance is based on the rigid body system, the associated dynamics must be discussed. Because the target is rotating with an angular rate of about 3.5°/s, a standard formulation with Euler angles is not possible, because of the singularity in the equations. The common next step to solve this problem would be to use the four-element quaternion representation. However, it was found that the N matrix, that represents the rigid body kinematics in the INDI controller degenerates once the attitude exceeds ±180 ° of rotation (refer to Section IV.B). Therefore, an alternative approach was used to solve the problem. By observing the angular rates of a body about an axis, it is possible to derive the evolution of attitude about the same axis by simple integration. This virtually represents the Euler angles without the singularity, and will be referred to as *pseudo Euler angles* for the rest of the research. The kinematics of the rigid body system can be simply defined using the angular velocity. This gives:

$$\dot{\boldsymbol{\Theta}} = \begin{pmatrix} \dot{\phi} \\ \dot{\theta} \\ \dot{\psi} \end{pmatrix} = \begin{pmatrix} \omega_1 \\ \omega_2 \\ \omega_3 \end{pmatrix} \tag{24}$$

The dynamic EOM for pseudo Euler angles can be found using the Euler's dynamic equations of motion, given by:[18]

$$\boldsymbol{J\dot{\omega}} + \boldsymbol{\Omega J\omega} = \boldsymbol{M_c} \tag{25}$$

where $\boldsymbol{J}$ is the inertia matrix, $\boldsymbol{M_c}$ indicates the control torque and $\boldsymbol{\Omega}$ is the skew-symmetric matrix given by:

$$\boldsymbol{\Omega} = \begin{bmatrix} 0 & -\omega_3 & \omega_2 \\ \omega_3 & 0 & -\omega_1 \\ -\omega_2 & \omega_1 & 0 \end{bmatrix} \tag{26}$$

Equations (24) and (25) together define the guidance state, which is then used to compute the error against the state vector from the plant (the flexible system) as shown in Fig. A1. The error is used to compute the control moments, which are applied to the plant to achieve the final attitude. The control theory used to derive the control moments will be discussed in the next section.

B. Controller Design

A linear PD controller is still among the most widely used controllers for attitude control. These controllers are mostly used for problems where the steady state error is not zero. The control moment for this controller is defined using:

$$\boldsymbol{M_c} = -(\boldsymbol{K_p e} + \boldsymbol{K_d \dot{e}}) \tag{27}$$

where $\boldsymbol{K_p}$ and $\boldsymbol{K_d}$ are proportional and derivative gains respectively. $\boldsymbol{e}$ and $\boldsymbol{\dot{e}}$ are the error in state and the error in the state derivative. The error state $\boldsymbol{e}$ can be computed as the difference with the commanded attitude. Since the commanded attitude rate is zero, $\boldsymbol{\dot{e}}$ depends only on the actual angular rate.

As stated before, the Incremental Nonlinear Dynamic Inversion controller is an enhanced modification of NDI controller. In a spacecraft attitude control problem, where the dynamics are nonlinear and often changing from one operation to another, for a linear controller often a single set of gains is insufficient to ensure efficient control. In such a case, gain scheduling needs to be done to adapt these gains according to the operations. However, by using a nonlinear feedback controller like NDI (or INDI), the need for gain scheduling can be eliminated and closed-loop stability is ensured. Another motivation for using the INDI controller is for the verification of the inertia modelling for the multibody system. Since the model works on inverse dynamics, which is influenced by the inertia of the body, any mismatch in inertia modelling will introduce a steady state error in the response of the system once it is stabilised. This validates the modelling of rigid-body inertia in the flexible multibody system and also, serves as a measure for inaccuracies in the mass inertia modelling.

An NDI controller typically consists of two loops. The outer loop linearises the system introducing a virtual control $\boldsymbol{v}$, which is used in the inner loop. The control moment is then obtained using:

$$\boldsymbol{M_c} = \boldsymbol{M^{-1}(x)(v - l(x))} \tag{28}$$

where $\boldsymbol{M(x)}$ and $\boldsymbol{l(x)}$ depend on the state variables ($\boldsymbol{x}$), and together they define the inverse dynamics of the system. A detailed description of the controller can be found in Ref. 17. The PD controller is used as the outer loop linear controller, which makes the virtual control ($\boldsymbol{v}$).

In cases where the dynamic models are very complex, dynamic inversion becomes difficult and may lead to incorrect results. Therefore, an alternative approach of INDI alters the structure of NDI in such a way that only a small part of the model is used and the model mismatch is minimised.[17] The final dynamic case is approximated by a first order Taylor series. With the notation "0" indicating the nominal case, the dynamics can be approximated by:

$$\boldsymbol{\dot{\omega}} \approx \boldsymbol{\dot{\omega}_0} + \frac{\boldsymbol{\partial \dot{\omega}}}{\boldsymbol{\partial \omega}}(\boldsymbol{\omega - \omega_0}) + \frac{\boldsymbol{\partial \dot{\omega}}}{\boldsymbol{\partial u}}(\boldsymbol{u - u_0}) \tag{29}$$

where the partial derivatives are evaluated at $\boldsymbol{\omega = \omega_0, u = u_0}$. The first term of the equation is the angular acceleration obtained from onboard sensors. For high sampling rates, when the difference between new and current angular acceleration becomes small, the equation can be further reduced. The partial derivative with respect to the state, i.e., the second term can be neglected. Therefore, the equation becomes

$$\boldsymbol{\dot{\omega}} \approx \boldsymbol{\dot{\omega}_0} + \frac{\boldsymbol{\partial \dot{\omega}}}{\boldsymbol{\partial u}}(\boldsymbol{u - u_0}) \tag{30}$$

The second partial derivative can be found from the dynamic equation of motion, Eq. (25), which is simply found to be $\frac{\boldsymbol{\partial \dot{\omega}}}{\boldsymbol{\partial u}} = \boldsymbol{J^{-1}}$. Using the notation $\boldsymbol{\Delta M_c = u - u_0}$ and re-arranging Eq. (30), we get:

$$\boldsymbol{\Delta M_c} = \boldsymbol{J(v - \dot{\omega}_0)} \tag{31}$$

The virtual control term ($\boldsymbol{v}$) is computed using a PD controller with dynamic inversion, which is applied in two loops. This is to obtain a Time Scale Separation in the inversion of dynamics, which allows quicker control. The outer loop is defined by:

$$\dot{\boldsymbol{x}}_{\boldsymbol{2}} = \boldsymbol{N}\boldsymbol{u}_{\boldsymbol{2}} \tag{32}$$

where $\boldsymbol{x}_{\boldsymbol{2}} = \boldsymbol{\theta}$, $\boldsymbol{u}_{\boldsymbol{2}} = \boldsymbol{\omega}$ and $\boldsymbol{N}$ is a matrix used for dynamic inversion of the plant given by Eq. (24). It can be defined as the coefficient matrix that establishes the relation between the rate of change of attitude, $\dot{\boldsymbol{\Theta}}$ with the angular rates of the system, $\boldsymbol{\omega}$. From Eq. (24), it can be concluded that $\boldsymbol{N}$ becomes an identity matrix for this formulation.

Going back to the outer loop, the virtual control is defined by the error in attitude (as compared to commanded) and the proportional gain.

$$\boldsymbol{v}_{\boldsymbol{2}} = -\boldsymbol{K}_{\boldsymbol{p}}\boldsymbol{e} \tag{33}$$

This is used by the outer loop to get the first control vector $\boldsymbol{u}_{\boldsymbol{2}}$,

$$\boldsymbol{u}_{\boldsymbol{2}} = \boldsymbol{N}^{-\boldsymbol{1}}(\boldsymbol{v}_{\boldsymbol{2}}) \tag{34}$$

This control vector $\boldsymbol{u}_{\boldsymbol{2}}$, is then fed as a reference to compute the virtual control again in the inner loop, it is given by:

$$\boldsymbol{v} = -\boldsymbol{K}_{\boldsymbol{d}}(\boldsymbol{x}_{\boldsymbol{1}} - \boldsymbol{u}_{\boldsymbol{2}}) \tag{35}$$

This can be substituted into Eq. (31) to obtain the change in control effort (ΔM_c) The final control torque is given by:

$$\boldsymbol{M}_{\boldsymbol{c}} = \boldsymbol{M}_{\boldsymbol{c,0}} + \boldsymbol{\Delta M}_{\boldsymbol{c}} \tag{36}$$

Having discussed the theory for the two controllers used in this research, the simulation results can now be analysed.

V. Results

The end goal of the research is to analyse the controllability characteristics of a chaser spacecraft performing two stages (synchronisation and connected phase) of Active Debris Removal (ADR) with a large uncontrolled target with flexible appendages. The control of the spacecraft is modelled using a linear PD controller and a nonlinear INDI controller. All analysis will be performed assuming ideal sensors. The control effort will be limited to ±50 Nm as specified by ESA.[12] Since the controller design remains elementary for a very dynamic model, three sets of target states will be analysed. The first set is a more challenging case of the target debris tumbling with an angular velocity of 3.5 °/s about all axes. In the second case, an angular velocity of 1.5 °/s about all axes is controlled. And lastly, an angular velocity of 3.5 °/s about Z-axis only, which is the nominal case given by ESA is considered. The used integration method is a high-order, variable-coefficient Ordinary Differential Equation solver, with fixed-leading-coefficient implementation, originally part of the NetLib mathematical library.[19] The dynamics is simulated with a step size of 10^{-3} s and the controller is sampled at 100 Hz. A zero-order hold is used to retain the present control moments, until the current time step matches the control frequency. The controllability strategy used to analyse both phases of the e.deorbit mission is stated below:

1. *Synchronisation*: In the synchronisation phase, the chaser has to match the rotational state and attitude velocity of the target, assuming it is already at the vicinity of the target and starting from zero angular velocity (about all axes). So, the initial state of the chaser is given by $\boldsymbol{x}_{\boldsymbol{cha}} = [0,\ 0,\ 0,\ 0,\ 0,\ 0]^T$, in the order of angular velocities followed by the pseudo Euler angles. For this phase, the control of the worst-case scenario, *i.e.,* the synchronisation with 3.5 °/s about all axes will be attempted first. If the system is successfully controlled by both controllers (PD and INDI), the other (easier) cases will not be attempted. Two control strategies will be perform for synchronisation. They are:

    - *Full state control*: The control of all the six states will be executed using the PD and INDI controller. In other words, the controller will correct for the errors in angular rates and attitude simultaneously.
    - *Rate control + Full state control*: To avoid saturation of the controller, it will be split into two components, *i.e.,* a rate (proportional) controller that operates until the angular rate has reduced below a pre-defined threshold, after which the full state control will be achieved using PD and INDI.

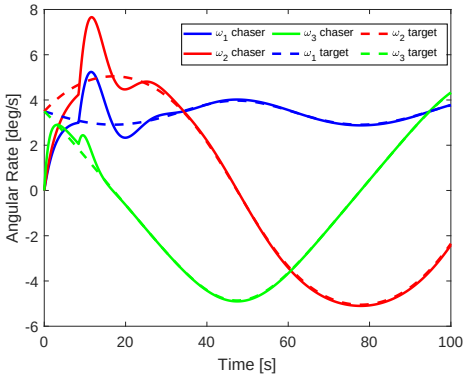

(a) Angular rates

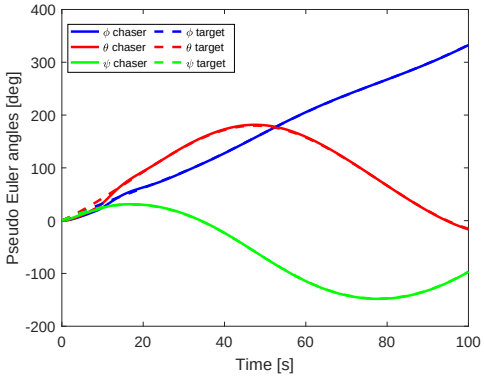

(b) Pseudo Euler angles

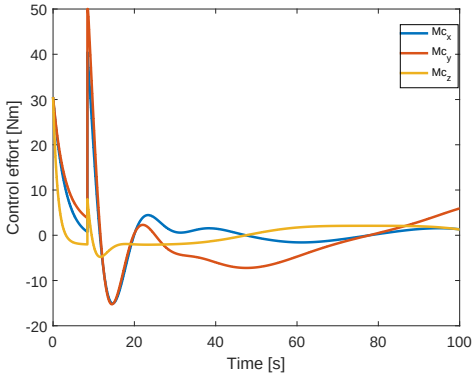

(c) Control effort

Figure 10. Control response of the flexible system using PD control

2. *Connected*: Since the dynamics of the stacked system has large asymmetries in inertia and flexible geometry, the control problem is more challenging. For this case, if the control moment limit of ±50 Nm does not result in stabilisation of the system, a sensitivity study will be performed with other control limits of ±10 Nm, ±25 Nm, ±100 Nm will be performed. While different angular rates will be analysed for this phase, the initial attitude for each case will be assumed to be zero. Some typical operations associated with deorbiting of a satellite will be analysed for this phase. This includes:

   - *Detumbling:* Detumbling is associated with the control problem of reducing the angular velocity from the current value to zero. This involves only a proportional rate control, and the full state PD and INDI will not be used here.
   - *Detumbling + reorientation:* This operation involves a combined control of the angular rates as well as the attitude, which results in detumbling and reorientation to a specified attitude for the final deorbitation manoeuvre. Full state control with PD and INDI will be performed for this operation.
   - *Reorientation:* In this operation, the goal is to achieve a specified attitude for deorbitation manoeuvre. It is assumed here that the detumbling has already been performed and the initial angular rates are zero. This is also achieved through full state control with PD and INDI controllers.

Hence, in this chapter the final results for the dynamics and control of the flexible multibody system will be analysed. Some simulation results from rigid-body control will also be presented as a benchmark. The results will be discussed in two parts as per the phases of the e.deorbit mission. In Sec. V.A, the simulations from the synchronisation phase will be summarised. In Sec. V.B, the same will be done for the connected phase.

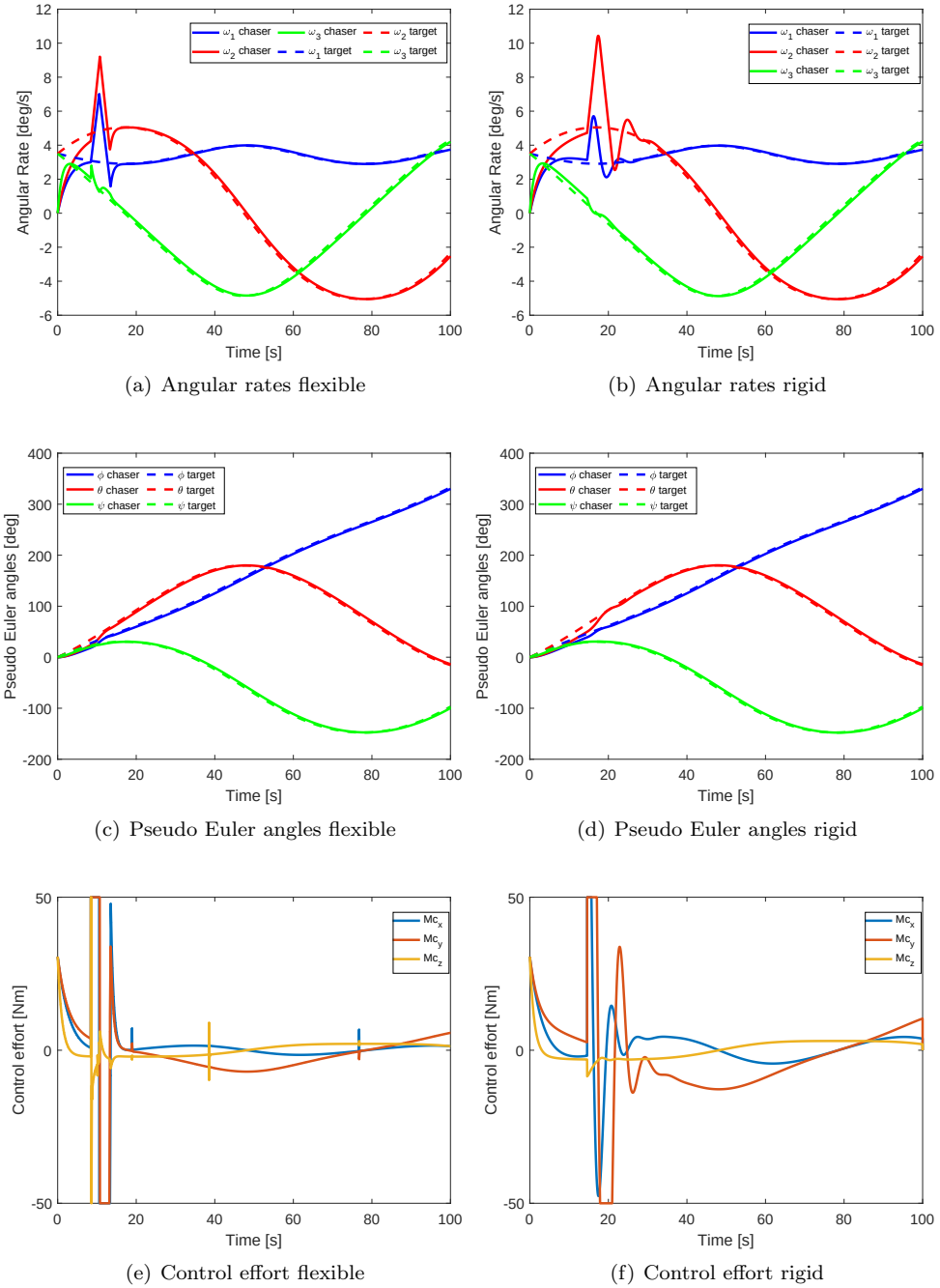

(a) Angular rates flexible

(b) Angular rates rigid

(c) Pseudo Euler angles flexible

(d) Pseudo Euler angles rigid

(e) Control effort flexible

(f) Control effort rigid

Figure 11. Control response of the flexible and rigid system using INDI control for synchronisation

A. Synchronisation

From the initial simulations, it was found that synchronisation using full state control did not lead to stability. This is because the relatively high angular rate of 3.5 °/s about all axes cannot be achieved when attitude control is also performed simultaneously. The (very large) attitude error drives the controller to correct it, slowing the rate control down and drives the system away from achieving the rate. The second option of rate control until a certain threshold and then switching to full control gives valuable results and will thus be discussed in further detail.

Figure 10 shows the response of the flexible multibody system to the PD controller based on rigid body system. It can be seen that the system has reached the required attitude and achieved steady state. Clear

Table 2. Summary of different detumbling and reorientation simulations.

Intial angular rate	$\omega = 3.5$ ° [all axes]			$\omega = 1.5$ ° [all axes]			$\omega = 3.5$ ° [Z-axis only]		
$\lvert M_{c,max} \rvert$	± 25	± 50	± 100	± 25	± 50	± 100	± 25	± 50	± 100
		[Nm]			[Nm]			[Nm]	
Rate control[P controller]	FAIL	FAIL	FAIL	FAIL	FAIL	FAIL	FAIL	FAIL	FAIL
Full state control [PD controller]	FAIL	FAIL	FAIL	FAIL	FAIL	FAIL	FAIL	FAIL	FAIL
Full state control [INDI controller]	FAIL	FAIL	FAIL	FAIL	FAIL	FAIL	FAIL	FAIL	FAIL
Rate + Full state control [PD controller]	FAIL	FAIL	FAIL	FAIL	FAIL	FAIL	FAIL	FAIL	FAIL
Rate + Full state control [INDI controller]	FAIL	FAIL	FAIL	FAIL	FAIL	FAIL	FAIL	FAIL	FAIL

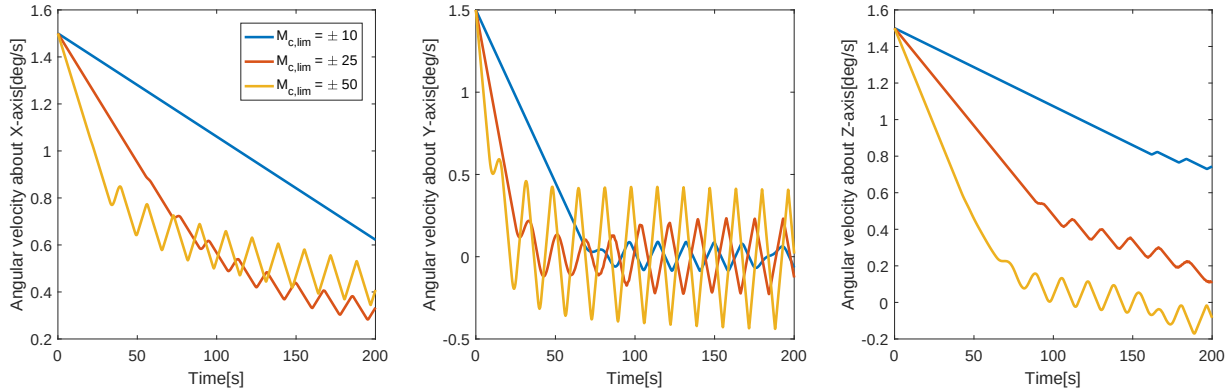

Figure 12. Angular rate sensitivity to different control moments for detumbling

effect of the solar panel vibrations cannot be observed in any of the attitude states, so it can be concluded that the chaser solar panel does not suffer from large vibrations. The angular rates suffer from some overshoot (see Fig. 10(a)) due to the switching from rate to full control, but is quickly stabilised. The pseudo angle errors do not suffer from large errors or overshoots (see Fig. 10(b)). Lastly, the control saturates only at the moment of control switching (see Fig. 10(c)). The rest of the response remains smooth.

Figure 11 shows the performance of INDI for the rigid and flexible models during synchronisation. For the same gains, the flexible model seems to give a better performance. This may be a result of the switch from rate control to full control happening sooner in the flexible model. There is a small steady state error seen in both flexible and rigid body models. This is possibly due to integration errors accumulating over time, since the incremental controller almost acts like an Euler integration on control effort. Also, finer gain tuning might eliminate these errors. Since the same steady state error is found in both models, it is verified that the rotational inertia was modelled correctly for the multibody system. Again no oscillations are observed due to flexible elements, confirming that the perturbations for the chaser satellite alone are low and can be handled by the controller. The INDI controller shows faster convergence to steady state as compared to PD.

B. Connected

Multiple simulations were performed for the connected state, as it was stated in the introduction. Table 2 summarises the simulations performed using different control strategies. It clearly indicates that none of the control strategies were robust enough to detumble the stacked configuration. This is because the braking manoeuvres performed to decrease the angular rates cause vibrations in the solar panel. This further causes an error in state, which the controller attempts to correct, resulting in more oscillatory braking action. This just aggravates the oscillation of the flexible system. Hence the stack fails to achieve the commanded state.

Since the angular rate control is the main cause of the excitation in the flexible parts, using lower control moments for control of the angular rate should yield better stability. A sensitivity study performed on rate control confirms the explanation. It can be seen from Fig. 12 that the controller with the smaller control limits of ± 10 Nm induced the least vibrations. However, the small oscillations are still not eliminated.

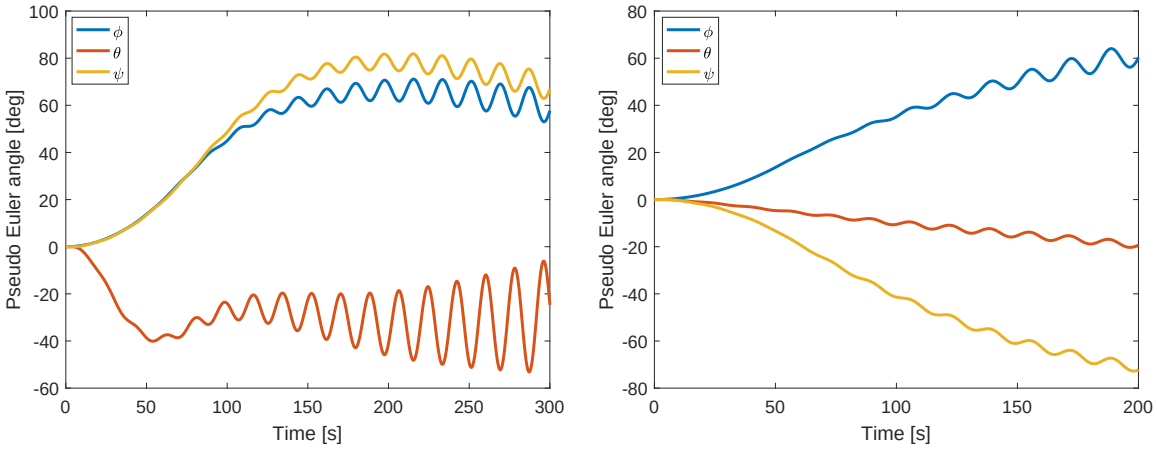

(a) PD controller (50° -30° 60°)

(b) INDI controller (50° -30° -60°)

Figure 13. Reorientaion using PD and INDI controllers

It would require some structural damping or an advanced control system to obtain steady state.

Lastly, Fig. 13 shows the performance of the two controllers for reorientation to a specified point for deorbiting, assuming the stack has already detumbled. The control is performed using smaller maximum moments of ±25 N. It can be observed that the oscillations start as attitude gets closer to the commanded value, again due to the braking of angular velocity. Another observation that can be made is that the INDI controller induces smaller oscillations as compared to the PD controller. This proves that the (non-linear) INDI controller works better for the more dynamic and uncertain models.

VI. Conclusions and Recommendations

In this paper, the dynamics and control associated with a chaser satellite synchronising with a large target debris with flexible appendages, and detumbling the docked configuration is modelled and analysed. A new floating frame formulation based on absolute interface coordinates is used to model the complex flexible multibody dynamics. The control is performed using a linear PD control and an Incremental Nonlinear Dynamic Inversion (INDI) controller. As a test case target debris, the configuration of Envisat is used. The large, eight tonne space debris with a 14.2 m long solar panel, is assumed to be tumbling with an angular rate of 3.5 °/s about all axes, which makes the dynamics very nonlinear and complex.

The satellite's flexible components were modelled using beam elements connected to each other at the interface points. The rigid body mass and inertia properties were captured in the multibody system using lumped masses. With the new floating frame formulation the constraints were applied without the use of Lagrange multipliers. Additional, model reduction was also performed using the new method to minimise computation time. In the control system, the guidance is based on the rigid body model of the system, and the flexible multibody model is used as the plant. This means that elastic vibrations due to the large appendages are treated as external perturbations to the system.

On analysis it was found that the new floating frame multibody approach provided a good balance between computation time and accuracy, which is optimal for control simulations. During the synchronisation phase, both linear and nonlinear controllers successfully achieved steady state with good accuracy. However, for detumbling of the stacked configuration with a large flexible appendage, the flexible dynamics dominated due to large vibrations in the solar panel and both controllers failed to achieve steady state. Nonetheless, the INDI controller shows better performance compared to PD, which destabilises quickly. The chosen controls can be concluded to be too elementary for the complex nonlinear dynamics associated with the stacked configuration.

For future research, more control strategies can be developed to understand the extent of controllability of the nonlinear dynamics of the system. For instance, a sequential single axis control can be performed. Also, the control stability can be analysed using an advanced controller. In the structural dynamics, damping and other quadratic velocity inertia terms (like centrifugal stiffening), can be added. Modelling the flexible

body inertia can also be improved using inertia shape integrals. Lastly, an analysis can be performed on the elastic energy stored in the flexible appendages for a better understanding of the dynamics and to facilitate better control.

Acknowledgements

The authors of the paper would like to express their gratitude towards Marcel Ellenbroek, Jurnan Schilder and Koen Dwarshuis, from the University of Twente, for their support throughout the research.

References

[1]Ellenbroek, M.H.M. and Schilder, J., "On the use of absolute interface coordinates in the floating frame of reference formulation for flexible multibody dynamics", *Multibody system dynamics*, pp. 1-16, Springer 2017.

[2]Singh, S., "Multibody approach to the controlled removal of large space debris with flexible appendages", Masters thesis, Delft University of Technology, 2019.

[3]Wasfy, T.M. and Noor, A.K.,"Computational strategies for flexible multibody systems", *Applied Mechanics Reviews*, Vol. 56, No. 6, American Society of Mechanical Engineers, 2003.

[4]Craig, R.R., and Bampton, M.C.C., "Coupling of substructures for dynamic analysis", AIAA Journal, 6(7), 1313-1319, 1968.

[5]Schilder, J.P., Ellenbroek, M.H.M. and de Boer, A., "Superelements in a minimal coordinates floating frame of reference formulation." IMSD, Lisbon, Portugal, 2018.

[6]Meirovitch, L., "Computational Model of Structural Dynamics", *Sijthoff and Noordhoff*, The Nederlands, 1980.

[7]van de Wetering, B, "Velocity forces and mass terms in new floating frame formulation", Masters Thesis, University of Twente, 2018

[8]Dwarshuis, K.S., "Geometric Stiffness Formulation for a Superelement", Masters Thesis, University of Twente, 2017.

[9]Jonker, J.B., "Dynamics of Spatial Mechanisms with Flexible Links", Ph.D. Thesis, Delft University of Technology, Netherlands, 1988.

[10]Cardona, A., "Superelements modelling in flexible multibody dynamics", Multibody Syst. Dyn. 4, 245 266, 2000.

[11]Virgili, Bastida, B., Lemmens, S. and Krag, H., "Investigation on Envisat attitude motion", ESA, ESOC, 2014.

[12]European Space Agency (ESA), "Concurrent Design Facility Study Report", 2012

[13]Habets, J. M. G., "Evolving Systems Approach to the Attitude Control of a Large Space Debris Removal Spacecraft", Masters Thesis, Delft University of Technology, 2015.

[14]Hassmann, C.H.G. and Fenili, A., "Attitude and vibration control of a satellite with a flexible solar panel using LQR tracking with infinite time", In: *Proceedings of the ASME International Congress of Mechanical Engineering*, 2007.

[15]Fufa, B., Zhao-Bo, C. and Wensheng, M., "Modeling and simulation of satellite solar panel deployment and locking", Information Technology Journal, 9(3), 600-604, 2010.

[16]Shabana, A.A., "Flexible multibody dynamics: review of past and recent developments", Multibody system dynamics, 1(2), pp.189-222., 1997.

[17]Sieberling, S., Chu, Q.P. and Mulder, J.A., "Robust flight control using incremental nonlinear dynamic inversion and angular acceleration prediction", Journal of guidance, control, and dynamics, 33(6), pp.1732-1742, 2010.

[18]Wie, B., "Space vehicle dynamics and control", American Institute of Aeronautics and Astronautics, 2018.

[19]Brown, P.N., Byrne, G.D. and Hindmarsh, A.C., "VODE: A Variable Coefficient ODE Solver," *SIAM J. Sci. Stat. Comput.*, Vol. 10, 1989, pp. 1038-1051.

Appendix A. Simulator Architecture

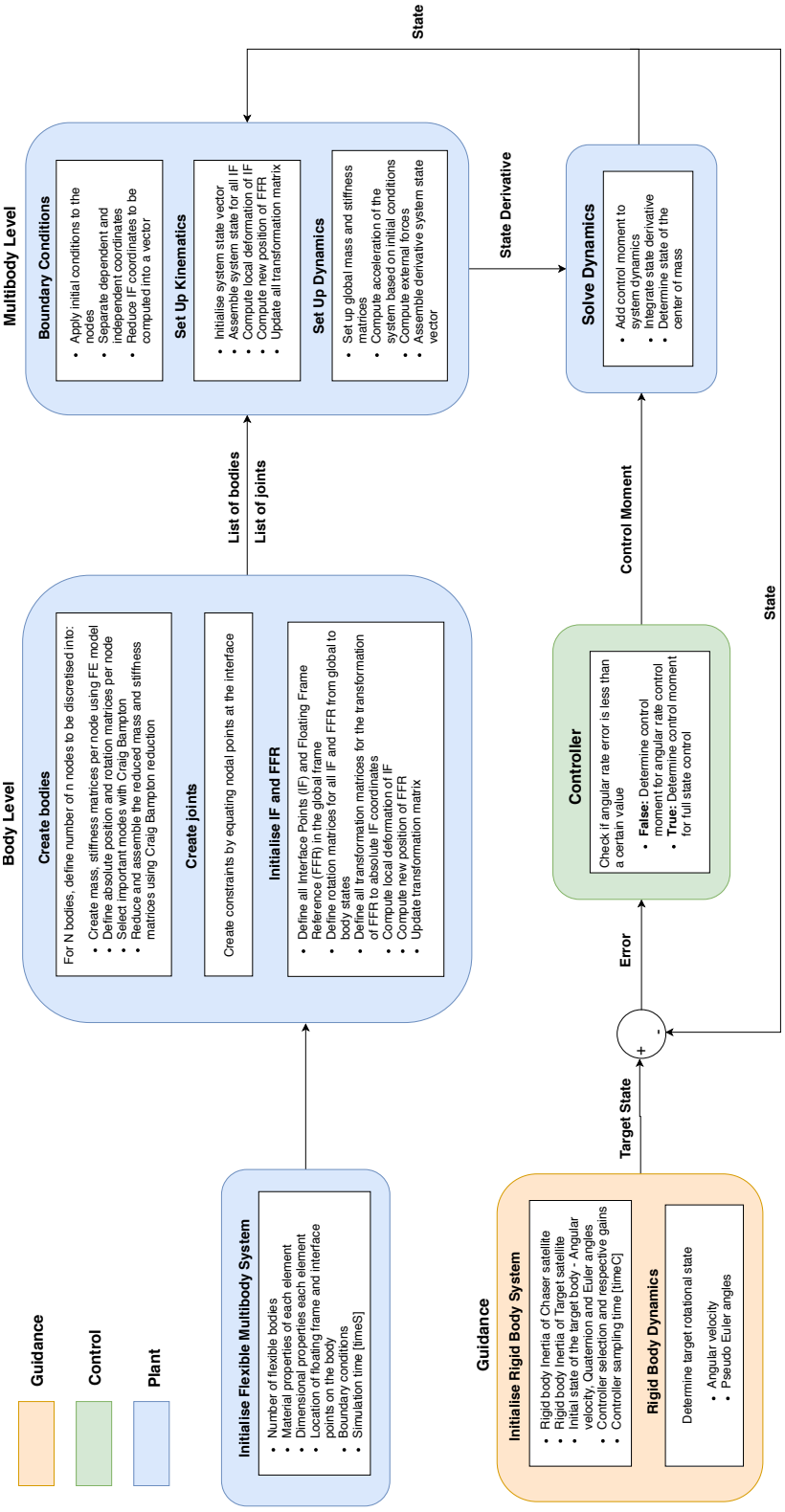

Figure A1. Simulator Architecture